13th International Symposium on Particle Image Velocimetry – ISPIV 2019
Munich, Germany, July 22-24, 2019

Unscented Kalman filter (UKF) based nonlinear parameter estimation for a turbulent boundary layer: a data assimilation framework

Zhao Pan[1,2*], Yang Zhang[1], Jonas P. R. Gustavsson[1], Jean-Pierre Hickey[2], Louis N. Cattafesta III[1*]

[1] FAMU-FSU College of Engineering, Florida Center for Advanced Aero-Propulsion, Tallahassee, FL, 32310, USA

[2] University of Waterloo, Department of Mechanical and Mechatronics Engineering, Waterloo, Ontario, N2L 3G1, Canada

[*] panzhao0417@gmail.com, lcattafesta@fsu.edu

Abstract

A turbulent boundary layer is an essential flow case of fundamental and applied fluid mechanics. However, accurate measurements of turbulent boundary layer parameters (e.g., friction velocity u_τ and wall shear τ_w), are challenging, especially for high speed flows (Smits et al., 2011). Many direct and/or indirect diagnostic techniques have been developed to measure wall shear stress (Vinuesa et al., 2017). However, based on different principles, these techniques usually give different results with different uncertainties. The current study introduces a nonlinear data assimilation framework based on the Unscented Kalman Filter that can fuse information from i) noisy and gappy measurements from Stereo Particle Image Velocimetry, a Preston tube, and a MEMS shear stress sensor, as well as ii) the uncertainties of the measurements to estimate the parameters of a turbulent boundary layer. A direct numerical simulation of a fully developed turbulent boundary layer flow at Mach 0.3 is used first to validate the data assimilation algorithm. The algorithm is then applied to experimental data of a flow at Mach 0.3, which are obtained in a blowdown wind tunnel facility. The UKF-based data assimilation algorithm is robust to uncertain and gappy experimental data and is able to provide accurate estimates of turbulent boundary layer parameters.

1 Introduction

Despite the advances of computational methods, the experimental determination of the parameters of a turbulent boundary layer (TBL), such as friction velocity (u_τ) and wall shear stress (τ_w), with low uncertainties still remains challenging, especially for high-speed flows (Smits et al., 2011). Over the years, various diagnostic techniques have been developed and can be classified into four groups as shown in Fig. 1 (Winter, 1979; Haritonidis, 1989; Naughton and Sheplak, 2002). These techniques are based on different principles and are characterized by distinct advantages/disadvantages. For example, Particle Image Velocimetry (PIV) is essentially non-intrusive but generally suffers from inadequate resolution near the wall, the Preston tube experiment is intrusive but relatively inexpensive to carry out. While modern micromachined shear stress sensors can potentially provide direct measurements of τ_w, their rigorous characterization is a topic of current research (Mills et al., 2017).

Indeed, high fidelity measurements close to the wall are in general difficult for both intrusive and non-intrusive techniques. Probes (e.g., hot-wires and Pitot tubes) perturb the flow and are sensitive to their placement (Örlü et al., 2010). Optical based near-wall diagnostics (e.g., PIV and Particle Tracking Velocimetry (PTV), Laser Doppler Velocimetry (LDV), etc.) are also difficult or even inaccessible due to reflections, sparse particle seeding density, and high flow gradients (Kähler et al., 2012). To address these problems, one approach is to fit or extrapolate the gappy (and often noisy) data from hot-wire anemometry or PIV to an analytical description of the TBL profile, such as Musker's or Spalding's profile (Pujals et al., 2010; Pabon et al., 2018) and the Clauser-Chart (Wei et al., 2005), or some modified versions of these classic

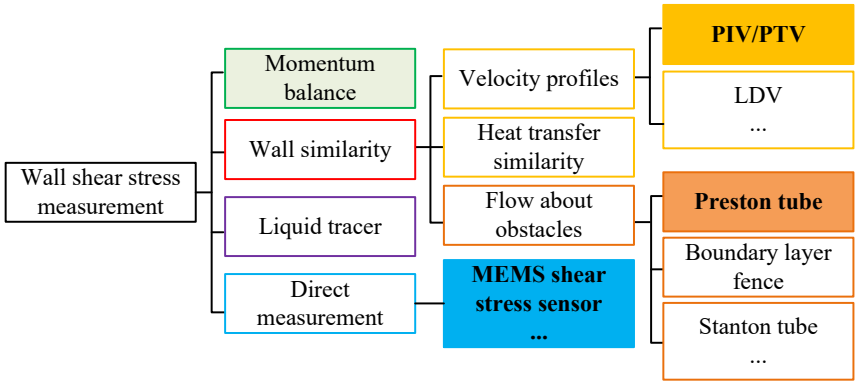

Figure 1: Outline of parameter measurement techniques for turbulent boundary layers (adapted from Winter (1979)). Techniques employed in the present research are highlighted in bold font.

TBL profile descriptions, which are applicable in the viscous sublayer and buffer layer region (Kendall and Koochesfahani, 2008; Örlü et al., 2010; Rodríguez-López et al., 2015).

A nonlinear fitting or regression algorithm commonly looks for a set of parameters in the theoretical expression that minimizes a norm (e.g., L^1- or L^2-norm) of the difference between a fitting function and (noisy) data from experiments. However, it is difficult for such a regression algorithm to directly provide uncertainties of the resulting parameters despite the fact that the experimental measurements typically have quantified uncertainties. In addition, a regression method often encounters the following challenges: namely the difficulty in i) overfitting to uncertain experimental data from multi-sensor diagnostic setups, where each sensor may have different levels and characteristics of uncertainties; ii) assigning appropriate weights or trust to different measurements (e.g., more trust in direct and/or high-fidelity measurements than that from noisy and/or indirect measurements); iii) faithfully taking higher-order information of the measurements into account (e.g., correlated uncertainty of velocity measurements from PIV); and iv) accounting for sensitivity to inaccurate determination of the wall position (Örlü et al., 2010).

To address the above four challenges, we first develop a data assimilation algorithm based on the Unscented Kalman filter (UKF, briefly introduced in §2) to estimate the TBL parameters (e.g., u_τ and τ_w). The nonlinear UKF is designed to fuse three data sets: i) velocity profiles measured with Stereo-PIV (SPIV), which leads to correlated uncertainties associated with a non-zero overlap of interrogation windows in the data processing; ii) differential pressure (and its uncertainty) measured by a Preston tube attached to the wall surface; and iii) a micromachined direct wall shear stress sensor and its uncertainty. The algorithm design is described in §3.

Next, we validate the UKF-based data assimilation algorithm, in §4, using composite data obtained from a high-fidelity numerical simulation of a flow at Mach 0.3, which is contaminated with artificial noise (both correlated and uncorrelated). The results indicate that the UKF-based TBL parameter estimation is robust and accurate. In addition, the approach naturally handles the aforementioned four challenges compared to traditional nonlinear regression methods by minimizing the estimated uncertainty of the unknown parameters in TBL profiles.

Last, the UKF-based data assimilation algorithm is applied to experimental data (§5) from a channel flow at Mach 0.3 obtained in a blowdown wind tunnel facility at Florida State University. This application is an example of a nonlinear Kalman filter based data assimilation framework, applied to fluid flow diagnostics for parameter estimation, which is flexible and can be potentially adapted to other measurement techniques and simulation results. Discussions and conclusions are provided in §6.

2 Unscented Kalman Filter

The UKF belongs to the family of Kalman filters, which is one of the most common tools for data assimilation, multi-sensor information fusion, and state/parameter estimation, etc., depending on the context of the field of application. A Kalman filter is commonly designed based on an analytical model of a dynamic process/system $\boldsymbol{X}_{k+1} = \mathcal{F}(\boldsymbol{X}_k, \boldsymbol{p})$, where $\boldsymbol{X}_k$ is the unknown state vector of the dynamic process at time step k, and the system dynamic model $\mathcal{F}(\cdot)$ is parameterized by $\boldsymbol{p}$. The model of the observable variables of

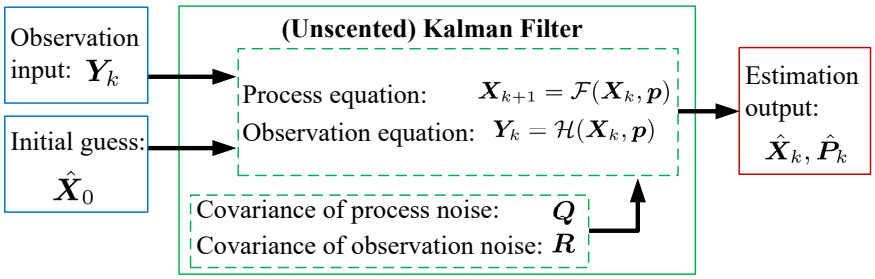

Figure 2: Kalman filter framework for state and/or parameter estimation.

the dynamic system is $\boldsymbol{Y}_k = \mathcal{H}(\boldsymbol{X}_k, \boldsymbol{p})$, where $\boldsymbol{Y}_k$ is the observation vector containing the variables that can be measured by transducers. The mapping between $\boldsymbol{X}_k$ and $\boldsymbol{Y}_k$ is modeled by $\mathcal{H}(\cdot)$. The inaccuracy of $\mathcal{F}$, which is considered via additive process noise, is modeled by a covariance matrix $\boldsymbol{Q}$. Similarly, the observation noise covariance matrix $\boldsymbol{R}$ models the uncertainty properties of observations of the system. Initializing the Kalman filter by an initial guess of the unknown state variables ($\hat{\boldsymbol{X}}_0$) and feeding the observations measured from transducers ($\boldsymbol{Y}_k$), the Kalman filter recursively outputs optimal estimation of the state variables ($\hat{\boldsymbol{X}}_k$) by minimizing the corresponding covariance, $\hat{\boldsymbol{P}}_k = \mathrm{cov}(\boldsymbol{X}_k - \hat{\boldsymbol{X}}_k)$. The diagonal elements of the $\hat{\boldsymbol{P}}_k$ can be considered as an uncertainty estimate of $\hat{\boldsymbol{X}}_k$. The framework of the Kalman filter is illustrated in Fig. 2, and the detailed algorithm derivation and applications of classic Kalman filters are well documented (e.g., Bishop et al. (2001)). The classic Kalman filter is designed for linear and Gaussian processes or systems. For a nonlinear system, the Extended Kalman filter (EKF) is a standard technique that embeds the first-order linearization of the nonlinear system in the Kalman filter framework. Thus, the estimation can be erroneous, especially when the noise is not Gaussian or the process is strongly nonlinear.

The unscented Kalman filter (UKF) is an extension to the Kalman filter, which uses a set of carefully chosen sample points around the state variables to statistically represent the dynamics of nonlinear system. These sample points are called sigma points, which are chosen to have the same mean and covariance as the corresponding state variable. Implementation details of the UKF can be found in, for example, Wan and Van Der Merwe (2000). These sigma points propagate through the nonlinear dynamic system and precisely carry the statistical information of variables (i.e., expected value and covariance). Compared to the EKF, the UKF is superior since it does not assume additive Gaussian noise in the observation and does not need to linearize the process model. For non-Gaussian observations, the UKF is accurate to at least the second-order moments (i.e., variance). In addition, the UKF is less expensive than typical particle methods (e.g., Monte Carlo methods), and it follows the same setup as a Kalman filter for state/parameter estimation (shown in Fig. 2). In the present research, we use the UKF to design a state-parameter estimation algorithm to fuse diagnostics from multiple sensors to determine the turbulent boundary layer parameters, such as wall shear stress and friction velocity.

3 Data assimilation algorithm based on the UKF

An UKF was designed to fuse the measurements from three different diagnostic techniques (Stereo-PIV, Preston tube, and shear stress sensor) to estimate the TBL parameters.

Velocimetry techniques, such as PIV, are commonly used to measure the mean velocity profile in a TBL. The mean velocity profile in a TBL can be explicitly described by Musker's profile, $u^+ = f(y^+)$, where $u^+ = u/u_\tau$, $y^+ = yu_\tau/\nu$, y is the coordinate perpendicular to the wall, ν is the kinematic viscosity of the fluid, and u_τ is the friction velocity. In physical units, the velocity profile can be expressed as

$$u(y) = f_1(y, u_\tau, \delta, \Pi, \nu) \quad 0 \le y < \delta, \tag{1}$$

which is parameterized by friction velocity u_τ, boundary layer thickness δ, and wake factor Π. Equation (1) is a representation of the velocity profile similarity near the wall, which is fairly long and omitted here for brevity. Its form, parameters, and derivation can be found in Musker (1979).

Another popular technique to measure skin friction is a Preston tube. A Preston probe is a pitot probe attached to the wall with a diameter small enough to capture the dynamic pressure in the inner part of the

boundary layer. The wall shear stress and friction velocity can be derived based on the measured dynamic pressure (Head and Rechenberg, 1962):

$$\log_{10}\left(\frac{\tau_w D^2}{\rho\nu^2}\right) = K_1 \log_{10}\left(\frac{\Delta P D^2}{\rho\nu^2}\right) - K_2, \tag{2}$$

where ρ is the density of the fluid, D is the outer diameter of the Preston tube, and ΔP is the measured dynamic pressure at the Preston tube. $K_1 = 0.889$ and $K_2 = 1.400$ are constants when $3.7 < \log_{10}\left(u_\tau^2 D^2/\nu^2\right) < 5.3$ is satisfied (Ferriss, 1965). The nonlinear function (2) maps the relationship between the unknown TBL parameter τ_w and the experimental observation (ΔP) through wall similarity of flow over an obstacle (Winter, 1979). Rearranging (2) leads to

$$\Delta P = f_2(\tau_w, \nu, D, \rho). \tag{3}$$

The wall shear stress can also be directly measured by a miniature floating-element shear stress sensor flush mounted in the wall and can be written as a function of friction velocity:

$$\tau_w = f_3(u_\tau) = \rho u_\tau^2. \tag{4}$$

The mean flow profile of a TBL must satisfy the no-slip boundary condition at the wall ($u|_{y=0} = 0$), which can be rearranged as

$$0 = u(0); \tag{5}$$

and the condition at the edge of the boundary layer, $u(y = \delta_{0.99}) \approx 0.99 U_\infty$, or

$$\delta_{0.99} \approx f_4(U_\infty), \tag{6}$$

where U_∞ and its location can be directly determined from velocity profile measurements by PIV.

Based on (1), (3) – (6), we could setup the observation function of the UKF as

$$\boldsymbol{Y}_k = \mathcal{H}(\boldsymbol{X}_k, \boldsymbol{p}) = \begin{pmatrix} f_1(y, u_\tau, \delta, \Pi, \nu) \\ f_2(u_\tau, \nu, D, \rho) \\ f_3(u_\tau, \rho) \\ 0 \\ f_4(U_\infty) \end{pmatrix}, \tag{7}$$

where $\boldsymbol{Y}_k = [u(y), \Delta P, \tau_w, 0, \delta_{0.99}]^T$ is the observation vector that is made up by the left hand side of (1), (3) – (6). $\boldsymbol{X}_k = [\tau_w, u_\tau, \delta, \Pi]^T$ are the (unknown) variables to be estimated, and $\boldsymbol{p} = [\nu, \rho, D]$ are the known parameters of the fluid and measurement setup. It is worth noting that τ_w in $\boldsymbol{Y}_k$ is the *known* shear stress measurement from the transducer, which is contaminated by *unknown* noise, while τ_w in $\boldsymbol{X}_k$ is the *unknown* true value of the wall shear stress to be estimated.

In the context of parameter-state estimation on the basis of a Kalman filter, the unknown parameters are typically treated as pseudo-states. Since the pseudo-states in $\boldsymbol{X}$ are TBL parameters and are considered time-invariant constants, the difference equation of the state vector is formulated as

$$\boldsymbol{X}_{k+1} = \mathcal{F}(\boldsymbol{X}_k) = \begin{pmatrix} \rho u_{\tau_k}^2 \\ \mathbf{diag}(0,1,1,1)\boldsymbol{X}_k \end{pmatrix}, \tag{8}$$

where $\mathbf{diag}(\cdot)$ denotes a diagonal matrix, and the elements, from left to right, are listed in the parentheses.

The covariance of process noise of corresponding TBL parameters is set to be a diagonal matrix $\boldsymbol{Q} = \mathbf{diag}(\sigma_{\tau_w}^2, \sigma_{u_\tau}^2, \sigma_\delta^2, \sigma_\Pi^2)$. The specific value of $\boldsymbol{Q}$ is determined by the order of magnitude and significant digits of $\boldsymbol{X}$. Specific examples can be found in §5.

The observation noise covariance is a *block* diagonal matrix:

$$\boldsymbol{R} = \begin{pmatrix} \boldsymbol{\sigma}_{PIV}^2 & & & & \\ & \sigma_{PT}^2 & & & \\ & & \sigma_{SSS}^2 & & \\ & & & \sigma_0^2 & \\ & & & & \sigma_\infty^2 \end{pmatrix}, \tag{9}$$

where $\boldsymbol{\sigma}^2_{PIV}$ is the covariance matrix of the velocity data measured using PIV, σ^2_{PT} is the variance of pressure measured from Preston tube, and σ^2_{SSS} is the variance of the shear stress sensor reading, respectively. PIV processing commonly employs overlapped interrogation windows; thus it leads to correlated uncertainty and/or noise in the results. Thus, $\boldsymbol{\sigma}^2_{PIV}$ is typically a banded matrix (e.g., tridiagonal or pentadiagonal, etc., matrix depending on the overlap ratio of the interrogation windows). The principal diagonal elements ($\sigma^2_{PIV_{i,i}}$) of $\boldsymbol{\sigma}^2_{PIV}$ represent uncertainties of PIV measurements at each vector, which can be evaluated by various methods (Sciacchitano et al., 2015), and the off-diagonal elements are not necessarily zero. Namely, the upper and lower diagonal elements ($\sigma_{PIV_{i,i\pm j}}, j = 1,2,...$) of $\boldsymbol{\sigma}_{PIV}$ are nonzero due to the overlapped interrogation windows of PIV measurements, which is one of the signature characteristics of PIV compared to other velocimetry techniques. However, this higher-order uncertainty information of PIV is rarely evaluated and applied when PIV is used (Wieneke, 2017). Finally, σ^2_0 and σ^2_∞ provide uncertainties in the boundary conditions, which are set to be small values, and further explanations are provided in §4.

Equipped with the above setup, the standard routine of the UKF as an state/parameter estimator is implemented (see Wan and Van Der Merwe (2000) and Fig. 2). The UKF gives robust and accurate estimation of the TBL parameters and the corresponding uncertainties based on the measurements from multiple diagnostic techniques.

4 Algorithm validation

To validate the UKF-based data assimilation algorithm, we constructed synthetic noisy and gappy data sets to mimic the measurements of SPIV, Preston tube, and a wall shear stress sensor based on a high fidelity direct numerical simulation (DNS) of a channel flow at Mach 0.3, which is used as the ground truth.

The DNS database of turbulent channel flow was generated to assess the data assimilation framework. The near wall velocity from these channel flow simulations represents a numerical analogue to the experimental boundary layer data. The scale-resolving simulations were computed using Hybrid, a high-order LES/DNS code developed by Larsson et al. (2013) and Bermejo-Moreno et al. (2013). A sixth-order central differencing scheme with high-order artificial dissipation is used to compute the spatial derivatives; the equations are advanced in time using a fourth-order, explicit Runge-Kutta scheme. The Reynolds number based on the friction velocity and channel half height is approximately 750 and the bulk Mach number is 0.3. Doubly periodic boundary conditions were applied to the stream- and span-wise directions; no-slip was imposed at the walls. The domain size is $2\pi \times 2 \times \pi$ and selected to allow an adequate representation of the mean flow characteristics (Lozano-Durán and Jiménez, 2014). The grid resolution was $512 \times 512 \times 340$ with a hyperbolic tangent stretching of the grid in the wall-normal direction; this resolution results in wall unit grid spacing of $dx^+ = 9.24$, $dy^+ = (0.1 - 7.5)$, and $dz^+ = 6.96$. The flow at the wall was resolved to $y^+ = 0.1$. The dimensional friction velocity of this DNS data was $u_\tau = 4.695$ m/s, and the boundary thickness $\delta_{0.99}$ is approximately 2.4 mm.

The mean DNS velocity profile near the wall was cropped to simulate the gappy SPIV measurements that have difficulties to resolve the buffer layer of a flow at Mach number 0.3. The synthetic PIV data were down-sampled to have similar spatial resolution as in the experiments (i.e., 36 vectors in the $55 \leq y^+ \leq 600$ range which spans over 1.8 mm in physical units). In practice, our PIV measurements close to the wall tend to have higher uncertainty due to finite reflections (e.g., see $z \approx -10$ mm near the wall in Fig. 6(B)) and low seeding density (e.g., $z \approx -10$ mm in Fig. 6(D)). We model these uncertainties by calculating the root-mean-square of $N = 500$ instantaneous uncertainty profiles ($\sigma_{PIV_{inst}}$) directly exported from DaVis software (LaVision, Germany) of the SPIV data set of a flow at Mach 0.3 (see Fig. 6, and more details can be found in §5). Thus, the values of the principal diagonal of $\boldsymbol{\sigma}^2_{PIV}$ were calculated as $\sigma^2_{PIV_{i,i}} = \sum_{i=1}^{N} \sigma^2_{PIV_{inst}}/N^2$. For example, $\sigma_{PIV}|_{y^+=55} = \sigma_{PIV_{1,1}} = 0.210$ m/s, is higher than the measurements near the edge of the boundary layer $\sigma_{PIV}|_{y^+=600} = \sigma_{PIV_{36,36}} = 0.126$ m/s. With a 75% overlap of the interrogation window being used in the PIV cross-correlation calculation and an triangle-like correlation profile of the correlation ($\sigma_{PIV_{i,i\pm j}} = (1 - j/4)\sigma_{PIV_{i,i}}$, $0 \leq j \leq 4$, Wieneke (2017); Howell (2018)), a Cholesky decomposition was used to generate Gaussian noise for the velocity profile ($\varepsilon_{u_{PIV_i}}$) whose (up to 6 closest) neighboring noise are correlated, where each measurement has an assigned variance (i.e., $\varepsilon_{u_{PIV_i}} \sim \mathcal{N}(0, \boldsymbol{\sigma}^2_{PIV})$). Adding this synthetic noise to the mean flow profile from the DNS, we emulate the noisy and gappy synthetic TBL profile measurement from the SPIV data (Fig. 3(C)).

Synthetic pressure measurement of the Preston tube was generated by measuring dynamic pressure of the DNS data at the center line ($y^+ = 46$, indicated by the purple arrow in Fig. 3(C)) of a virtual Preston tube with

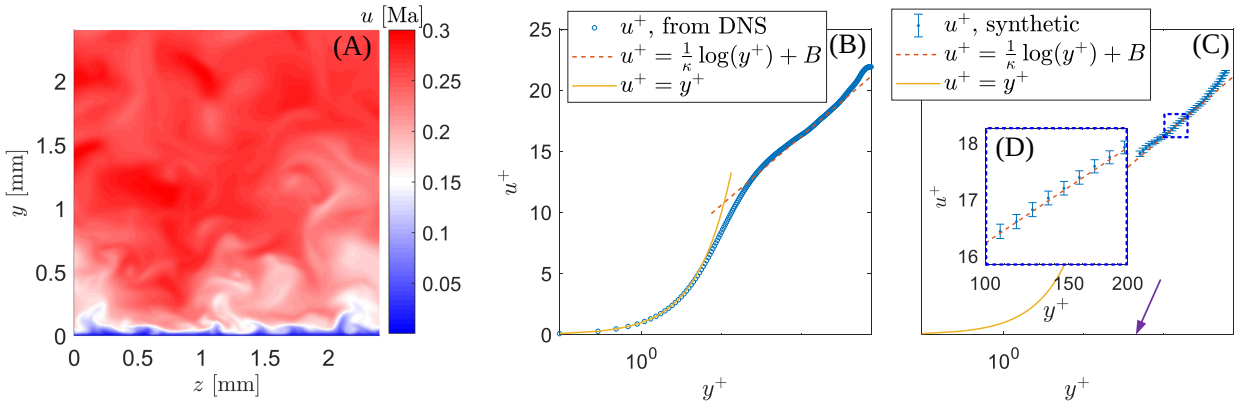

Figure 3: DNS data and DNS-based synthetic data. (A) A slice of the instantaneous velocity field snapshot from the DNS. (B) Mean flow profile (u^+) from the DNS data. The logarithmic law employs constants $\kappa = 0.41$ and $B = 5.0$ as reference. (C) Synthetic (gappy and noisy) SPIV data of mean flow profile. A zoomed-in view is shown in (D). Blue dots indicate the noisy and gappy mean flow profile, and the error bars indicate the corresponding uncertainties. The purple arrow indicates the location of the center line of the Preston tube.

an outer diameter $D = 0.30$ mm. The added noise was Gaussian ($\varepsilon_{PT} \sim \mathcal{N}(0, \sigma_{PT}^2)$, where $\sigma_{PT} = 0.01\Delta P$ is set to match the real Preston probe uncertainty described in §5). It is worth noting that this synthetic Preston tube measurement is ~7% lower than the nominal value according to τ_w from DNS based on (2).

Similarly, the shear stress sensor measurement was modeled by adding artificial noise to the exact value of τ_w calculated from the DNS data. We assumed that the shear stress sensor had high uncertainty with non-Gaussian distribution to challenge the data assimilation algorithm: $\varepsilon_{SSS} \sim \mathcal{U}(0, \sigma_{SSS}^2)$, where $\sigma_{SSS} = \tau_w/\sqrt{3}$, meaning that the sensor reading could be anywhere from 0 to $2\tau_w$, uniformly distributed. With ε_{PIV}, ε_{PT}, and ε_{SSS} added to the synthetic PIV measurements, Preston tube reading, and shear stress sensor measurements from the DNS data, respectively, we have the synthetic noisy experimental data as observation $\boldsymbol{Y}$ to be input to the UKF.

In addition, it should be noted that Musker's profile does not strictly satisfy the no-slip condition (i.e., $u = f_1(y = 0)$ is small but not zero), and the reading of $\delta_{0.99}$ is very sensitive to the measurements of U_∞. We therefore set small but non-zero values of the uncertainty of the boundary conditions at the wall and at the edge of the boundary layer: $\sigma_0 = 1 \times 10^{-3} u_\tau$, and $\sigma_\infty = 10^{-1}\delta_{0.99}$, respectively. This means that the data assimilation algorithm 'softly' enforces the boundary conditions. With the covariance ($\boldsymbol{\sigma}_{PIV}^2$) and variances ($\sigma_{PT}^2$ and σ_{SSS}^2) evaluated, the observation covariance matrix $\boldsymbol{R}$ is set up according to (9).

In practice, we do not know the exact value of the TBL parameters such as τ_w, u_τ, and Π *a priori*. However, a rough estimation, or even the order of magnitude, of the TBL parameters with a nonlinear fit method (e.g., Örlü et al. (2010)) is enough to set the last two parameters of the UKF, which are the process noise covariance ($\boldsymbol{Q}$) and the initial guess of the pseudo-states ($\hat{\boldsymbol{X}}_0$), respectively. For example $u_\tau \sim O(10^0)$ m/s for a flow at Mach 0.3, and we only keep four significant digits. Thus, $\sigma_{u_\tau} \approx 10^{-3}$ m/s is a reasonable estimation of the process noise to 'model' the inaccuracy of the *constant* parameter u_τ. Similarly, let $\boldsymbol{P} = \mathbf{diag}(10^1, 10^{-3}, 10^{-6}, 10^{-3})$, and choose an arbitrary initial guess of $\boldsymbol{X}_0$ such as $\boldsymbol{X}_0 = (10, 1, 10^{-3}, 1)$ to run the UKF to give an optimal estimate of the TBL parameters [1].

A typical data assimilation result is shown in Fig. 4. After several iterations, the UKF converges to optimal estimates of the TBL parameters. The wall shear stress (τ_w) and friction velocity (u_τ) are accurately estimated (red dashed line) with less than 0.5% and 0.1% relative error, respectively. The darker and lighter shades of red patches indicate the 1σ and 3σ uncertainty bands of the estimation. Despite that $\hat{\delta}$ has a bias error compared to the true value, the estimation of τ_w and u_τ, which are of more practical interests, are not significantly affected. This UKF-based data assimilation algorithm is robust to the wall offset (Δy) of PIV measurements. As shown in Fig. 5(A), $\hat{u}_\tau$ and $\hat{\tau}_w$ are mostly less than 1% and 3%, respectively, over a wide range of wall offset ($-10 \leq \Delta y/\delta_\nu \leq 10$, where δ_ν is the viscous length scale) for the simulated data of a flow at Mach 0.3. In this synthetic flow, $10\delta_\nu = 32.3$ μm in physical unit. As a reference, a

[1] Values of $\boldsymbol{Q}$ and $\boldsymbol{R}$ are in the units of [Pa, m/s, m, -].

typical 16×16 pixel interrogation window physical length in a real experiment (e.g., described in §5) is 0.208 mm, and 75% interrogation window overlap ratio leads to 52.0 μm grid spacing between neighboring PIV vectors. This algorithm is also robust to PIV (or potentially other velocimetry measurements) with low spatial resolution. Fig. 5(B) shows the relative error of $\hat{u}_\tau$ and $\hat{\tau}_w$ when spatial resolution of PIV is changed (from 80 vectors/mm, which is the original DNS data resolution in the range of $55 < y^+ < 600$, to 20 vectors/mm, which is similar to the experiments shown in §6, and to much coarser PIV data such as 5 or 2 vectors/mm). Even 3 vectors (corresponding to 2 vectors/mm in Fig. 5) from PIV measurements can lead to accurate $\hat{u}_\tau$ and $\hat{\tau}_w$ estimation with approximately 1% and 2% expected relative error, respectively. While spatial resolution higher than 20 vectors/mm may be difficult to achieve, it is still interesting to explore the influence of high spatial resolution. The results implies that, in practice, this data assimilation algorithm can be applied to velocimetry techniques having lower spatial resolutions than PIV.

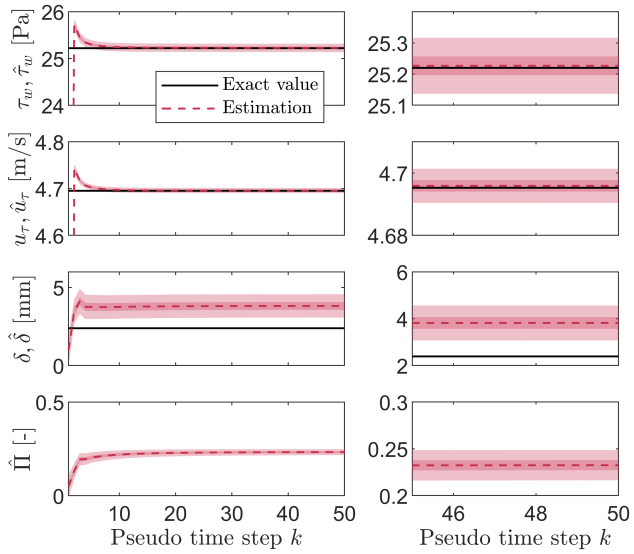

Figure 4: UKF estimation of TBL parameters. The black solid lines indicate the true values from DNS data. The red dashed lines are the estimation output from the UKF. The darker and lighter shades of red indicate the 1σ and 3σ uncertainty bands, respectively. The corresponding zoomed-in views are shown in the right column.

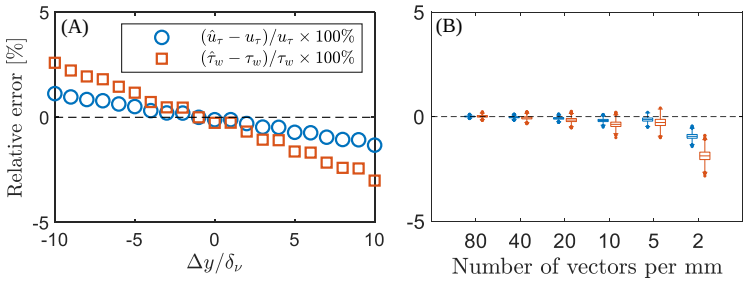

Figure 5: Relative error in the UKF-estimated wall shear stress and friction velocity, when (A) the synthetic PIV measurements are shifted by Δy in y-direction, and (B) the resolution of PIV measurements are varied. Each box in the grouped box plot in (B) contains 5000 independent runs of the UKF-based data assimilation algorithm. The blue and red boxes indicate the error in $\hat{u}_\tau$ and $\hat{\tau}_w$, respectively. The horizontal bar in the middle indicate the median, the upper and lower edge of the boxes are the 25% and 75% percentile, and the upper and lower whiskers indicate the $\pm 3\sigma$ bounds, respectively.

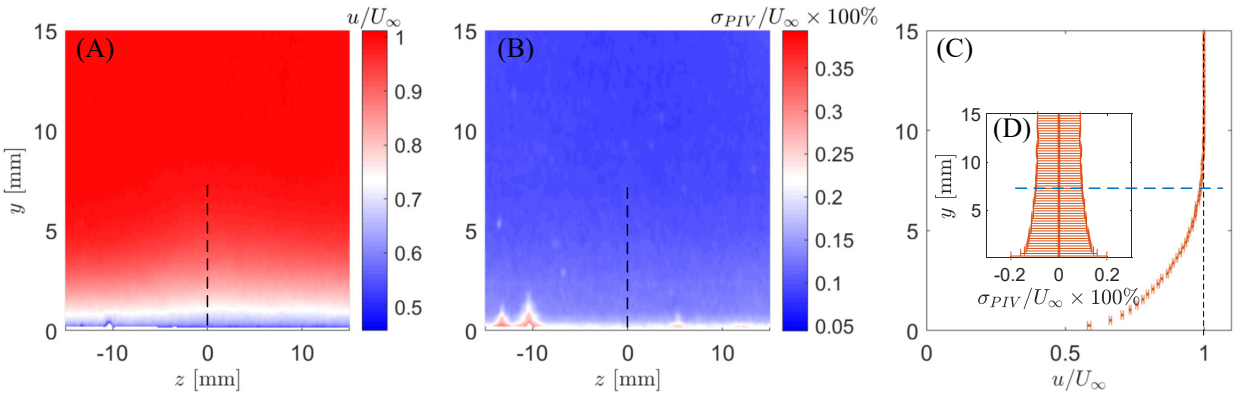

Figure 6: Averaged z-direction velocity profile (A) and uncertainty (B) from $N = 500$ snapshots of stereo-PIV (U_∞ is the free stream velocity). The black dashed line indicates where the data (shown in (C)) is sampled and used as input of the UKF algorithm and/or least square fit. Velocity profile $u(y)$ and the corresponding uncertainty ($\sigma_{PIV_{i,i}}$) are shown in (C) and (D), respectively. Only 1 out of 4 data points are shown for visualization. The blue dashed line indicates the edge of boundary layer ($\delta_{0.99}$).

5 Experiments and verification

In this section, we apply the UKF-based data assimilation algorithm to the experimental data sets. SPIV was used to measure the TBL profile in a channel flow at Mach 0.3. An optical system consisting of an Evergreen Nd:YAG laser (EVG00400), plano-convex lens and plano-concave cylindrical lens was used to produce a laser sheet with a thickness of approximately 2 mm at 10 Hz into the flow. Sub-micron (nominally 0.3 µm) diameter seeding particles were generated using Rosco fog fluid in a customized Wright nebulizer seeder and injected upstream of the stagnation chamber. Two Imager sCMOS cameras (2560 × 2160 pixels, LaVision) were used to acquire the image pairs. Each camera was equipped with a Nikon Micro-Nikkor 105 mm 1:2.8 lens, a Scheimpflug, and a 532 nm band-pass filter. All the PIV data and corresponding uncertainty quantification were acquired and processed using DaVis 8.4. A multi-pass interrogation window scheme from 48×48 pixels to 16×16 pixels was applied in the processing. This resulted in a resolution of 19 vectors/mm. The mean flow profile was calculated by averaging $N = 500$ instantaneous snapshots. The mean flow profile and the uncertainty profile are shown in Fig. 6(A) and (B), respectively. The PIV data used by the data assimilation algorithm is shown in Fig. 6(C).

Preston probe measurements were used to provide an independent measurement of friction velocity. Based on the range of validity of the correlation of Ferriss (1965) and data in Head and Rechenberg (1962), a probe with the outer diameter of 0.30 mm was chosen. This hypodermic tubing was attached in the streamwise direction with the tip at the streamwise location of an upstream static pressure tap in the test section. This static tap and the Preston probe were connected to a 5 psid (35 kPa) differential pressure transducer, PX26-005DV, and the measured differential pressure, ΔP, was used to calculate the local shear stress using Ferriss correlation based on the data by Head and Rechenberg (1962).

The direct shear stress measurements were carried out using a flush-mounted, micromachined floating-element sensor from IC^2, Type CS-A05, 300 Pa range. This model has a sensing element of 1×0.2 mm and a bandwidth of dc-5 kHz. In fact, the shear stress sensor measured significantly lower shear stresses than derived from other methods (Table 1). The bias was well beyond the nominal uncertainty and its origin is unknown. Thus, we model this bias by noise with uniform distribution, and the expected amplitude of the noise is the same to the scale of the shear stress sensor reading.

With the experimental data and the corresponding uncertainty from the SPIV, Preston tube, and the shear stress sensor, the UKF-based data assimilation algorithm gives optimal estimates of the u_τ and τ_w (Table 1). To verify these estimates, besides comparing (directly) measured values from shear stress sensor and Preston tube, we also estimated u_τ via a least-squares fit of the SPIV data to the logarithmic law ($u^+ = \frac{1}{0.41}\log y^+ + 5.0$, which holds when $30 < y^+$ and $y < 0.2\delta$ (Bradshaw and Huang, 1995)). The values of u_τ and τ_w are only slightly dependent on the range of the data used in the fit (Table 1).

An alternative method considers the flow in a rectangular control volume that is bounded by the wall and half wind tunnel height in y-direction, and the location of current SPIV plane and the location of another SPIV plane Δx apart along the stream. Applying the mass conservation and x-momentum equation, one can

Table 1: Cross verification of the measured and estimated turbulent boundary layer parameters.

	shear stress sensor	Preston tube	log-law fit from PIV [1]	UKF	control volume
u_τ [m/s]	3.20	4.34	4.12 – 4.14	4.155 $\pm$0.005	4.35 $\pm$0.17
τ_w [Pa]	11.71	21.55	19.42 – 19.61	19.752 $\pm$0.082	21.68 $\pm$1.51

[1] Values vary depending on range of data used in fitting.

calculate skin friction drag coefficient, and consecutively τ_w and u_τ (Cantwell, 2018). This analysis falls in the momentum balance category shown in Fig. 1 and Winter (1979). This is an averaged τ_w evaluation over Δz that is not dependent on any similarities, and is expected to be slightly different than the results from local measurements such as PIV and Preston tube. Monte Carlo simulations were then performed to estimate the corresponding uncertainty (Table 1). More details about the control volume method can be found in Gustavsson et al. (2019). We find that most of the measurement techniques give similar estimates or measurement of u_τ and τ_w, except the wall shear stress sensor.

6 Discussion and conclusions

The UKF-based data assimilation is a useful framework that can fuse multi-sensor diagnostics and output robust optimal estimates of TBL parameters. In contrast to a nonlinear regression method, which seeks parameters that minimize a chosen error norm, the UKF-based data assimilation method minimizes the covariance of the estimates. The data assimilation algorithm thus directly leverages uncertainty information of available experimental measurements. It is worth noting that the uncertainty or noise properties of the UKF are evaluated via covariance matrices, which naturally take higher order statistical information of measurements (e.g., PIV uncertainties are correlated) into account. By incorporating uncertainties of different diagnostic techniques, the UKF can systematically and objectively tolerate inaccurate measurements (e.g., shear stress sensor in the validation example in §4) and leverage measurements with lower uncertainty (e.g., SPIV in the validation example in §4).

The UKF-based data assimilation algorithm is also flexible. In the present studies, measurements and corresponding uncertainties of only PIV, Preston tube, and shear stress sensor were used. This is one example application of the UKF-based data assimilation framework. In fact, combination of other diagnostics, such as oil film, particle tracing velocimetry, boundary layer fence, etc., are also possible to be used to design new data assimilation algorithms for TBL parameter estimation. We leave these options for future work.

Acknowledgements

The computational time for the direct numerical simulations was supported by SciNet (www.scinethpc.ca) and Compute Canada (www.computecanada.ca).

References

Bermejo-Moreno I, Bodart J, Larsson J, Barney BM, Nichols JW, and Jones S (2013) Solving the compressible Navier-Stokes equations on up to 1.97 million cores and 4.1 trillion grid points. in *SC'13: Proceedings of the International Conference on High Performance Computing, Networking, Storage and Analysis*. pages 1–10

Bishop G, Welch G et al. (2001) An introduction to the Kalman filter. *Proc of SIGGRAPH, Course* 8:41

Bradshaw P and Huang GP (1995) The law of the wall in turbulent flow. *Proceedings of the Royal Society of London Series A: Mathematical and Physical Sciences* 451:165–188

Cantwell BJ (2018) *Fundamentals of Compressible Flow*. chapter 8. Stanford University

Ferriss DH (1965) *Preston tube measurements in turbulent boundary layers and fully developed pipe flow*. Her Majesty's Stationery Office

Gustavsson JPR, Zhang Y, Cattafesta L, and Kreitzman J (2019) Acoustic liner drag measurements. in *25th AIAA/CEAS Aeroacoustics Conference*. Delft, The Netherlands. AIAA Paper 2019-2683

Haritonidis JH (1989) The measurement of wall shear stress. in *Advances in fluid mechanics measurements*. pages 229–261. Springer

Head M and Rechenberg I (1962) The preston tube as a means of measuring skin friction. *Journal of Fluid Mechanics* 14:1–17

Howell JA (2018) *Distribution of Particle Image Velocimetry (PIV) Errors in a Planar Jet*. Master's thesis. Utah State University

Kähler CJ, Scharnowski S, and Cierpka C (2012) On the uncertainty of digital PIV and PTV near walls. *Experiments in fluids* 52:1641–1656

Kendall A and Koochesfahani M (2008) A method for estimating wall friction in turbulent wall-bounded flows. *Experiments in Fluids* 44:773–780

Larsson J, Bermejo-Moreno I, and Lele SK (2013) Reynolds- and Mach-number effects in canonical shock-turbulence interaction. *Journal of Fluid Mechanics* 717:293321

Lozano-Durán A and Jiménez J (2014) Effect of the computational domain on direct simulations of turbulent channels up to $Re_\tau = 4200$. *Physics of Fluids* 26:011702

Mills DA, Barnard C, and Sheplak M (2017) Characterization of a hydraulically smooth wall shear stress sensor for low-speed wind tunnel applications. in *55th AIAA Aerospace Sciences Meeting*. page 0478

Musker A (1979) Explicit expression for the smooth wall velocity distribution in a turbulent boundary layer. *AIAA Journal* 17:655–657

Naughton JW and Sheplak M (2002) Modern developments in shear-stress measurement. *Progress in Aerospace Sciences* 38:515–570

Örlü R, Fransson JH, and Alfredsson PH (2010) On near wall measurements of wall bounded flows – the necessity of an accurate determination of the wall position. *Progress in Aerospace Sciences* 46:353–387

Pabon RJ, Ukeiley L, Sheplak M, and Keane CB (2018) Characteristics of turbulent boundary layer large scale motions using direct fluctuating wall shear stress measurements. *Physical Review Fluids* 3:114604

Pujals G, Cossu C, and Depardon S (2010) Forcing large-scale coherent streaks in a zero-pressure-gradient turbulent boundary layer. *Journal of Turbulence* page N25

Rodríguez-López E, Bruce PJ, and Buxton OR (2015) A robust post-processing method to determine skin friction in turbulent boundary layers from the velocity profile. *Experiments in Fluids* 56:68

Sciacchitano A, Neal DR, Smith BL, Warner SO, Vlachos PP, Wieneke B, and Scarano F (2015) Collaborative framework for piv uncertainty quantification: comparative assessment of methods. *Measurement Science and Technology* 26:074004

Smits AJ, McKeon BJ, and Marusic I (2011) High Reynolds number wall turbulence. *Annual Review of Fluid Mechanics* 43:353–375

Vinuesa R, Örlü R, Discetti S, and Ianiro A (2017) Measurement of wall shear stress. *Experimental Aerodynamics; Discetti, S, Ianiro, A, Eds* pages 393–428

Wan EA and Van Der Merwe R (2000) The unscented Kalman filter for nonlinear estimation. in *Proceedings of the IEEE 2000 Adaptive Systems for Signal Processing, Communications, and Control Symposium (Cat. No. 00EX373)*. pages 153–158. IEEE

Wei T, Schmidt R, and McMurtry P (2005) Comment on the clauser chart method for determining the friction velocity. *Experiments in fluids* 38:695–699

Wieneke B (2017) *PIV Uncertainty Quantification and Beyond*. Ph.D. thesis. Delft University of Technology

Winter K (1979) An outline of the techniques available for the measurement of skin friction in turbulent boundary layers. *Progress in aerospace sciences* 18:1–57